Spectrochimica Acta Part A: Molecular and Biomolecular Spectroscopy 216 (2019) 236–248

Contents lists available at ScienceDirect

Spectrochimica Acta Part A: Molecular and Biomolecular Spectroscopy

journal homepage: www.elsevier.com/locate/saa

Weathering behavior of cinnabar-based tempera paints upon natural and accelerated aging

K. Elert *, C. Cardell

Department of Mineralogy and Petrology, Faculty of Science, University of Granada, Fuentenueva S/N, 18002 Granada, Spain

ARTICLE INFO

Article history:
Received 22 November 2018
Received in revised form 6 March 2019
Accepted 10 March 2019
Available online 12 March 2019

Keywords:
Historic pigments
Egg yolk
Pigment-binder interaction
Particle size
Photo-aging tests
Spectroscopic analyses

ABSTRACT

The darkening process of cinnabar and vermilion-based paint surfaces as well as pigment-binder interactions upon weathering have been studied by subjecting egg-yolk tempera dosimeters to UV-aging, RH cycling, and 2-year outdoor weathering with and without direct exposure to rain and sunlight. X-ray photoelectron spectroscopy proved that photooxidation resulted in Hg enrichment in the cinnabar pigment surface of weathered paints exposed to direct sunlight and rain, which caused important binder loss as well as thermal-induced crack formation and severe darkening of the unprotected pigments. Remarkably, darkening occurred in the absence of halogens and all pigments, independent of their preparation process (ground minerals or synthesis by a wet-process), were affected. After UV-aging, RH-cycling, and outdoor weathering in the absence of direct sunlight and rain, in contrast, pigments were still covered by egg yolk and did not undergo significant alteration. The binder, however, suffered important conformational and physical changes, including crack formation. These changes were significantly influenced by the size of the pigment. Additionally, XRD results indicate the presence of metacinnabar as an impurity in the original cinnabar and vermilion pigments, which might have been mistakenly identified as an alteration product in previous studies.

1. Introduction

Cinnabar, mercury (II) sulfide (HgS), has been a widely used pigment throughout history. It has been mined since the Neolithic age and its earliest use as a pigment dates back to 7000–8000 BCE in wall paintings at the Neolithic site of Catahöyük in Turkey [1]. Other important early decorative uses include Chinese pottery and Asian lacquerware, applications on human remains in Mayan Tombs [2], in murals in Pompeii [3], and on polychrome carpentry from the Nasrid period at the Alhambra palaces [4]. The pigment was very appreciated in the Middle Ages, Renaissance, and Baroque and can be found in many important paintings for example by Jan van Eyck, Titian, Rembrandt, or Rubens [5].

In general, the pigment is considered to be resistant to acids and alkalis and does not react with other pigments or binders [6]. However, it is photosensitive and a darkening of the pigment has been described when used in different binding media such as lime [3], oil, and tempera [7]. Different mechanisms responsible for the darkening have been proposed: a) transformation of red hexagonal α-cinnabar into black metacinnabar [8,9], a theory which has been questioned more recently [3,10,11]; b) formation of an alteration layer containing mercury chlorides and/or mercury sulfochlorides [3,7,10,12]; and c) photochemical redox reaction of HgS into Hg^0 and S^0, catalyzed by halogens at high RH and sunlight/UV exposure [13,14]. A number of researchers [10,15–18] suggest that the cinnabar's observed photosensitivity would depend on the pigment's preparation process/chemical composition and that impurities would trigger darkening under light exposure. In the vast majority of studies the critical role of halogens in the blackening of cinnabar is highlighted based on the presence of chlorine compounds (i.e., calomel, terlinguaite, eglestonite, corderoite, and kenhsuite) detected in the pigments´ alteration layer, which are often considered as intermediate products of the chlorine-induced degradation of cinnabar [3,7,11,14,19,20]. However, most of these chlorine compounds are whitish or light-colored and do not explain the black discoloration of cinnabar [3].

Several studies suggest that the photo-induced darkening is produced by the formation of an amorphous phase [10], possibly metallic mercury and that halogens would act as catalysts in this reaction [11,12,14,18]. Dreyer [15], in a pioneering study, also proposed that a layer of colloidal mercury would be responsible for the blackening of cinnabar. More recently, Anaf et al. [13] were able to demonstrate the formation of metallic mercury and the simultaneous release of SO_4^{2-} on laser-exposed, electrochemically treated (pretreatment in 1 M NaCl solution) HgS/Pt electrodes. However, the process leading to the formation of metallic mercury in their experiments was very different from

* Corresponding author.
E-mail address: kelert@ugr.es (K. Elert).

https://doi.org/10.1016/j.saa.2019.03.027
1386-1425/

the alteration (darkening) process undergone by paint upon natural or accelerated aging and, so far, the presence of a metallic mercury layer on blackened cinnabar paint has not been confirmed [11,13,18,20].

In an effort to further the knowledge on the weathering mechanisms of HgS-based paints, dosimeters were exposed to various aging tests. In order to evaluate the effect of different environmental parameters separately, dosimeters were subjected to 1-month RH-cycling under light exclusion, 1000 h UV exposure at low RH, and long-term outdoor testing with and without direct sunlight exposure. Observed changes in pigments and binders were correlated with different environmental factors, considering pigment-binder interactions and pigment particle size.

2. Materials and methods

2.1. Materials

In this study, natural cinnabars (color index PR 10677766) of different particle sizes from the Hunan district in China (Kremer Pigmente GmbH & Co. KG, Germany) and vermilion from Almadén, Spain (Caremi, Spain) were included. Note that cinnabar commonly refers to the natural mineral, whereas the synthetic form of the pigment is called vermilion [5]. The color of the pigment changes with particle size. Generally, coarse cinnabar (CIN-M and CIN-C) has a slightly bluish shade, while finely ground cinnabar has a more reddish-orange color as can be observed in the case of the Chinese cinnabar (Table 1). The fine grained vermilion from Almadén, however, shows a bluish-red color similar to that of the coarser pigments. According to the supplier (Kremer), the Chinese cinnabar is treated with a diluted organic binder solution during the separation of different particle sizes in a process similar to the method developed by Price [21]. However, no detailed information on the separation process and the employed organic compounds are available from the supplier and attenuated total reflection – Fourier transform infrared (ATR-FTIR) spectroscopy did not allow an unambiguous identification of the organic additive.

Tempera paints were prepared using fresh egg yolk as a binder. Egg yolk was chosen because it has been identified as a binder in historic polychromies of many monuments in Granada [4,22]. Egg yolk contains about 31.8–35.5 wt% lipids, 15.7–16.6 wt% proteins, 1.1 wt% ash, and 0.2–1.0 wt% carbohydrates. Its elemental composition, besides C, H and O, includes K, P, Ca, and Mg in concentrations ≤1 wt%, and S, Fe, and Na in concentrations ≤0.1 wt% [23].

2.2. Paint dosimeters preparation

The paints used in this study were prepared according to traditional procedures used by medieval painters, considering organoleptic parameters [24–26]. In order to obtain paint with an adequate consistency, the binder content was adapted to the demand of the differently graded pigments used here. The consistency was found adequate when droplets formed at the tip of the brush would not fall off easily. In order to prepare the egg tempera, the egg yolk was separated from the egg white and the chalazae. Afterwards, the skin was removed and the beaten egg yolk was directly mixed with the pigments.

Table 1
Characterization of commercial HgS-pigments.

Commercial pigment reference	Stereomicroscope image of pigments	Pigment size according to supplier	Pigment acronym
Cinnabar, dark No. 10628 (Kremer) Provenance: Hunan district, China	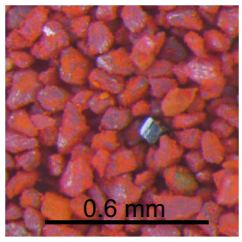	63–100 μm	CIN-C Cinnabar coarse
Cinnabar, medium No. 10627 (Kremer) Provenance: Hunan district, China	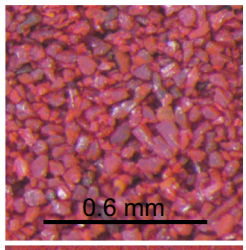	50–63 μm	CIN-M Cinnabar medium
Cinnabar, very fine No. 10624 (Kremer) Provenance: Hunan district, China	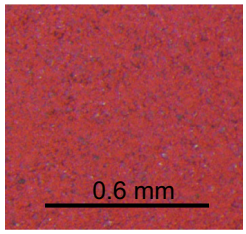	<20 μm	CIN-EF Cinnabar extra fine
Vermilion, genuine PR 106, (Caremi Pigmentos) Provenance: Almadén, Spain	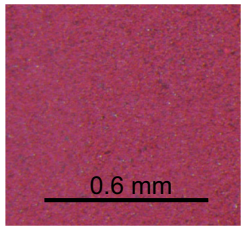	Not available	VER-ST Vermilion standard

To prepare the dosimeters, several paint layers were applied by brush on glass slides. Subsequent paint layers were only applied when the previous was completely dry. To obtain the egg yolk binder dosimeters, the pure binder was directly applied onto glass slides. Paint dosimeters were 20 × 15 × 1 mm in size. The paint layer was 0.07 ± 0.03 and 0.15 ± 0.03 mm in the case of fine (CIN-EF and VER-ST) and coarse-grained (CIN-M and CIN-C) paints, respectively. Paint samples were labeled by the letter EY for egg yolk. Letters RH, UV, A, and CC indicate exposure to RH cycling, UV exposure, and 2-year exposure at the Alhambra and in the city center of Granada (Spain), respectively.

2.3. RH cycling

RH cycling (RH was changed from 25 to 85 wt% at 12 h intervals) under light exclusion was performed in a climatic chamber (KMF115, Binder, Germany) at 25 °C for one month.

2.4. UV-aging

The UV aging test was performed during 1000 h using a continuously operated tubular UV lamp (G30T8, Sylvania, UK). The lamp emits >85 wt% of its energy in the UV-C wavelength range with a peak at 253.7 nm (1.1 W/m^2 at 1 m UV-C irradiance). During testing, paint dosimeters were placed in a ventilated chamber at 24 ± 3 °C and 25 ± 10 wt% RH. Day-light was excluded using aluminum foil.

2.5. Outdoor exposure test

Paint dosimeters were exposed to outdoor conditions in two locations in Granada, namely in the "Patio del Harem", a semi-open courtyard of the Alhambra palaces and on the first-floor balcony of a residential building in the city center (Realejo). At the Alhambra, dosimeters were placed in a niche and, thus, protected from direct sunlight and rain. Dosimeters placed in the city center faced a highly trafficked street, being exposed to the direct action of rain and sunlight ~5 h in winter and ~10 h in summer facing SE. The overall sunlight exposure duration was estimated to be ~5800 h at an irradiance level of ~1090 W/m^2 [27,28].

During outdoor testing, maximum *T* in summer and minimum *T* in winter were 40 °C and −3 °C, respectively, with diurnal variations of up to 20 °C. Average RH ranged from ~40 wt% in summer to ~75 wt% in winter, with diurnal variations of up to 50 wt%. Average precipitation was ~5 mm in summer and ~40 mm in winter [29].

2.6. Analytical techniques

2.6.1. Granulometry

The particle size of pigments was measured with a laser particle size analyzer (Mastersizer 2000LF, Malvern Instruments, UK). Samples were dispersed in ethanol.

2.6.2. Microscopy

Textural, morphological, and chromatic features of blank and aged paint dosimeters were studied using a stereomicroscope (SMZ 1000, Nikon, Japan) and a polarized light optical microscope (Jenapol-V, Zeiss, Germany).

2.6.3. X-ray diffraction (XRD)

The mineralogical composition of HgS-pigments and paint dosimeters was determined using an X-ray diffractometer (X'Pert PRO PANalytical B.V., The Netherlands). All analyses were performed using Cu-Kα radiation, Ni filter, 45 kV voltage, 40 mA intensity, 3° to 60° 2θ exploration range, and 0.05° 2θ s^1 goniometer speed. Identification of minerals was carried out using Xpowder software [30].

2.6.4. Thermogravimetric analysis (TG)

The egg yolk binder content of paint dosimeters was verified using a Shimadzu TGA-50H (Shimadzu, Japan) in flowing air (100 ml/min) at a constant heating rate of 10 °C min^{-1} (25–350 °C). According to our TG data, weight loss due to thermal decomposition of cinnabar/vermilion was not important below 350 °C (i.e., weight loss at $T \leq 350$ °C = 1.07 ± 0.18 wt%) and the observed weight loss in paints can primarily be attributed to organic binder degradation. The calculation of the binder content of dosimeters was performed considering the weight loss of the corresponding cinnabar or vermilion pigment and pure egg yolk in the same temperature range.

2.6.5. Spectrophotometry

Color changes of dosimeters before and after exposure to UV, RH, and 2-year outdoor exposures were determined with a portable spectrophotometer (CM-700d, Minolta, Japan) using illuminant D65, 10° observer, and Ø 6 mm measurement area. Data were expressed in CIE L*a*b* and CIE L*C*h color spaces (i.e., L* is luminosity or lightness which varies from black with a value of 0 to white with a value of 100; a* varies from +a* (red) to −a* (green) and b* from +b* (yellow) to −b* (blue), and C* is chroma or saturation. Color changes for L*, a*, b*, C*, and ΔE* were calculated. The latter was calculated using the following formula: $\Delta E^* = \sqrt{(\Delta L^*)^2 + (\Delta a^*)^2 + (\Delta b^*)^2}$. Note that calculations are only based on SCI (specular component included) values because the difference between SCI and SCE (specular component excluded) measurements was negligible. Average values are based on a minimum of 5 measurements per samples. Generally, a color differences of ΔE* ≥3 will be perceptible to the human eye [31].

2.6.6. Attenuated total reflection–Fourier transform infrared spectroscopy (ATR-FTIR)

ATR-FTIR spectroscopy was performed on blank and aged dosimeters using a Jasco 6200 (JASCO Analytical Instruments, Japan). Paint dosimeters were directly pressed against the ATR diamond crystal window. Pure pigments and binder (i.e., egg yolk), in contrast, were analyzed as powders. Infrared spectra were recorded at a 2 cm^{-1} resolution over 75 scans from 400 to 4000 cm^{-1}.

2.6.7. X-ray photoelectron spectroscopy (XPS)

An Axis Ultra-DLD (Kratos Analytical Ltd., U.K.) was used to determine the quantitative elemental composition and the oxidization state of Hg in cinnabar pigments and in the alteration layer of outdoor (city center of Granada) exposed dosimeters. Analysis was performed using monochromatic AlK$_\alpha$ radiation with a pass energy of 160 (survey scans) and 20 eV (high resolution scans). The analyzed area was ~300 × 700 μm in size. The C1s transition at 284.6 eV was used as reference to determine binding energies of Hg^0 and HgS. Ion-etching depth profiles were obtained using Argon for various periods of time (4 keV energy, 10 mA emission current). Note that it was not possible to measure the ablation depth achieved during ion-etching using scanning electron microscopy or atomic force microscopy as a result of the sample's high surface roughness (i.e., the relatively small impact of <1 μm depth caused by ion-etching could not be distinguished from surface imperfections on pigment particles ~50 μm in size). Thus, a nominal etch depth was determined using a calibration standard (i.e., Ta foil with a 60 nm Ta oxide layer), which was etched under identical conditions as the samples to be analyzed. The calculated nominal etch rate was 0.75 nm/min.

2.6.8. Field emission scanning electron microscopy (FESEM)

An Auriga (Carl Zeiss, Germany) coupled to an INCA-200 EDS was used to study morphological features and determine the chemical composition of carbon coated pigments and dosimeters. Working conditions: 10^{-4} Pa vacuum, 3 kV beam accelerating voltage in secondary electron imaging mode and 10 kV in backscattering imaging mode/microanalysis.

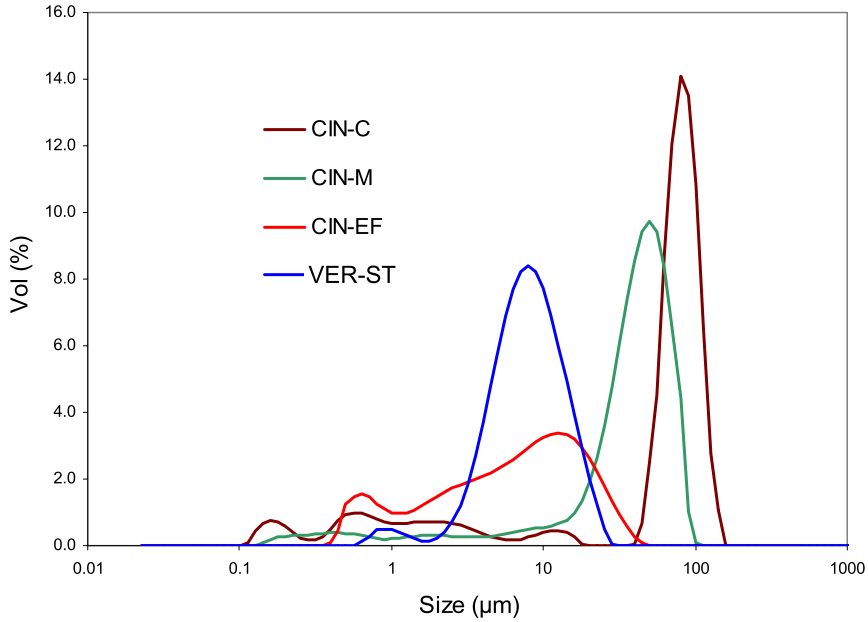

Fig. 1. Particle size distribution of cinnabar/vermilion pigments.

High-resolution X-ray maps from selected areas of uncoated samples (1 × 0.75 mm, 1024 × 768 pixels, 100 frames, 10 ms dwell time, 2.5 h acquisition, 3 nA filament current, and 20 eV/ch resolution) were obtained using a Supra 40Vp (Carl Zeiss, Germany) equipped with an Aztec 3 EDS and X-Max 50 mm detector. Working conditions: 40–66 Pa vacuum and 20 kV beam accelerating voltage. Quantitative data are based on sum spectra of the selected areas.

3. Results and discussion

3.1. Pigment characterization

3.1.1. Particle size analysis

According to particle size analyses (Fig. 1, Table 1 – Supplementary materials), pigments had a wider particle size range as compared to manufacturer's data. Pigments CIN-C, CIN-M, and VER-ST had a well-defined primary particle size maximum (i.e., 75, 48, and 8 μm, respectively) with a small contribution of smaller-sized particles ≤1 μm, whereas CIN-EF was constituted of particles with a broader particle size distribution, a primary particle maximum at 13 μm, and a relative large contribution of small particles ≤1 μm. Particle size is an important parameter, which does not only determine the pigments color and saturation, but might also influence pigment-binder interactions [32].

3.1.2. Morphological features

FESEM images of fine grained pigments revealed significant morphological differences between CIN-EF and VER-ST. The former showed particles of a relative wide size range with irregular edges/fractured appearance, typical for pigments obtained by grinding of bigger lumps (Fig. 2a). The latter, in contrast, was comprised of well-defined rhombohedral (tabular or prismatic) crystals of more uniform size (Fig. 2b), characteristic for synthetic pigments obtained by a wet-process [5,33]. Note that the wet-process consists of the conversion of the impure black mercury sulfide into vermilion by heating in an ammonium or potassium sulfide solution [5]. Overall, these morphological differences will have an important influence on the paints´ surface finish.

3.1.3. Mineralogical composition

According to X-ray diffraction data, the cinnabar and vermilion pigments used in this study matched JCPDS standard 060256. Pigments, generally, were of high purity. Only the coarsest pigment (CIN-C) contained a significant amount of quartz (Joint Committee on Powder Diffraction Standards (JCPDS) card n° 830,539), detectable with this technique. Actually, quartz is known as one of the gangue minerals associated with cinnabar [5]. XRD patterns of paints prepared with VER-ST and CIN-C revealed a shoulder at 2.92 Å (Fig. 3), which might correspond to the 200 Bragg peak of metacinnabar (JCPDS card n° 020453)

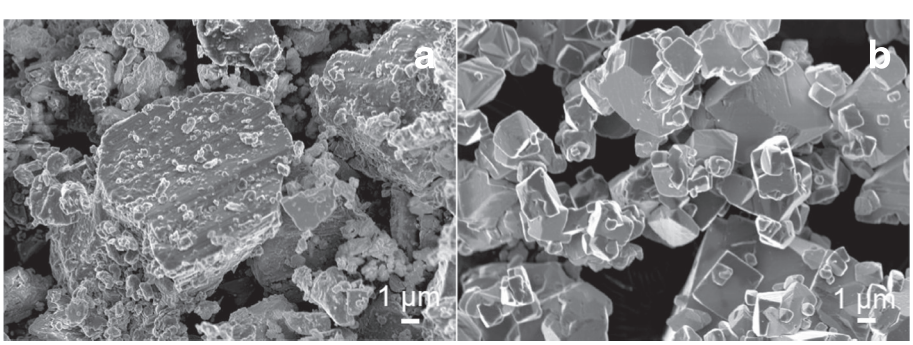

Fig. 2. FESEM images of cinnabar and vermilion pigments a) CIN-EF and b) VER-ST.

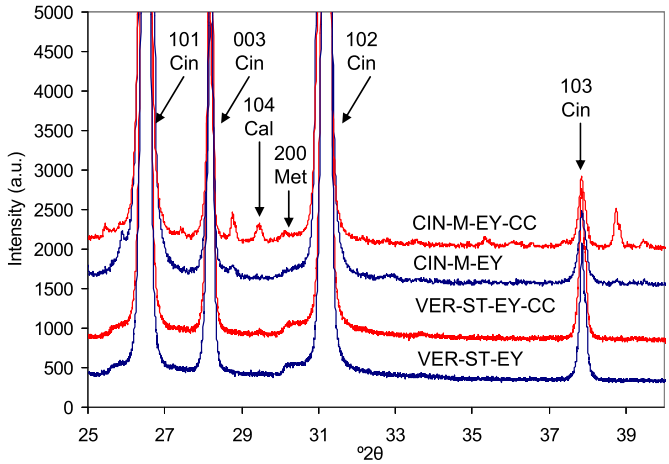

Fig. 3. XRD patterns of an unaltered VER-ST-EY dosimeter and a dosimeter exposed in the city center for 2 years. CIN = cinnabar, VER = vermilion, Cal = calcite, and Met = metacinnabar.

and hint its presence in the unaltered pigments. Note that metacinnabar has been reported as an impurity in cinnabar from Almadén [34,35] as well as from the Hunan province [36]. In the case of the synthetic vermilion from Almadén used in this study, it is unclear whether metacinnabar could also be a relict of the synthesis process [33]. The shoulder remained unchanged in the case of the outdoor-exposed, darkened cinnabar and vermilion-based paints, suggesting that solid state transformation of cinnabar to metacinnabar did not take place, and that it can thus not be held responsible for the observed darkening after 2 years of outdoor exposure. Considering these results, the question arises whether metacinnabar detected in darkened cinnabar paints in previous studies might have been mistakenly regarded as an alteration product instead of an impurity already present in the original cinnabar pigment. As mentioned above, only in a few cases, the transformation of red β-cinnabar into black α-cinnabar has been held responsible for the blackening of cinnabar [8,9]. However, the scientific proof for the presence of black α-cinnabar in the cited studies was either based on indirect evidence or called into question by the authors themselves. The XRD results presented here suggest that metacinnabar is most likely an impurity already present in the original pigment.

FESEM back scattered imaging in parallel with EDS allowed the identification of various impurities (Fig. 4). Numerous crystals were detected, which contained Si, Fe, Zn, or Ba. Their elemental composition

Table 2
Egg yolk binder content (wt%) of paint dosimeters calculated based on TG data.

Paint dosimeters	Egg yolk
CIN-C-EY	13.3
CIN-M-EY	14.3
CIN-EF-EY	23.4
VER-ST-EY	17.5

is compatible with the following minerals: Quartz (SiO_2), pyrite/marcasite (FeS_2), zinc blende (sphalerite, ZnS), and barite ($BaSO_4$). All these minerals are commonly found associated with cinnabar ores [5,17] and are, thus, not the result of a later addition during pigment processing.

3.2. Paint characterization

3.2.1. Binder content

Thermogravimetric (TG) analysis revealed that the binder content was directly related with the pigment particle size. Paints prepared with coarser pigments (CIN-C and CIN-M) contained less binder than paints prepared with the finer grained pigments in order to obtain adequate consistency (Table 2). The relatively high binder demand of CIN-EF was likely related with its particle size distribution. In the case of CIN-EF, 20.7 vol% corresponded to particles <1 μm, while VER-ST only contained 1.8 vol% of particles <1 μm. These results are in agreement with previous findings, showing that the binder demand increases as the pigment grain size decreases [37].

3.2.2. Surface morphology of paints

The surface morphology differed depending on the pigment grain size used for its preparation. Paint surfaces prepared with fine pigments (Fig. 5a) showed less severe crack formation than paints prepared with coarse pigments (Fig. 5b). Apparently, the finer grained pigment facilitated a more homogeneous binder distribution and, thus, reduced crack development caused by volume changes of the binder upon drying. Interferometric profilometry data have shown that surface roughness generally increased with increasing pigment grain size [38]. Additional crack formation will certainly further increase the surface area of paints prepared with coarse pigments. This is an important consideration, because surface soiling is directly related with surface roughness. Moreover, the organic and inorganic particle matter accumulated in cracks can enhance or catalyze chemical and physical attack.

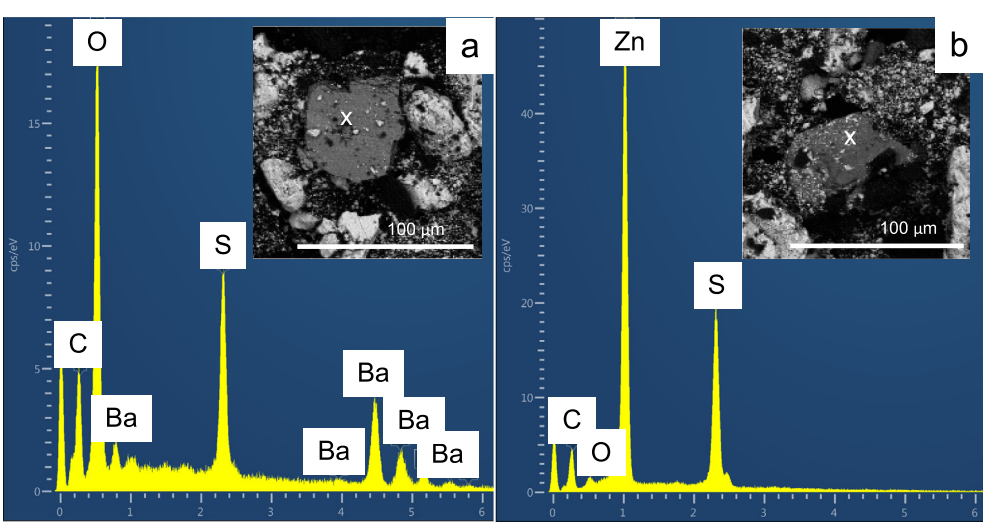

Fig. 4. FESEM backscattering images and corresponding microanalyses showing a chemical composition compatible with a) barite and b) zinc blende in dosimeters prepared with CIN-C.

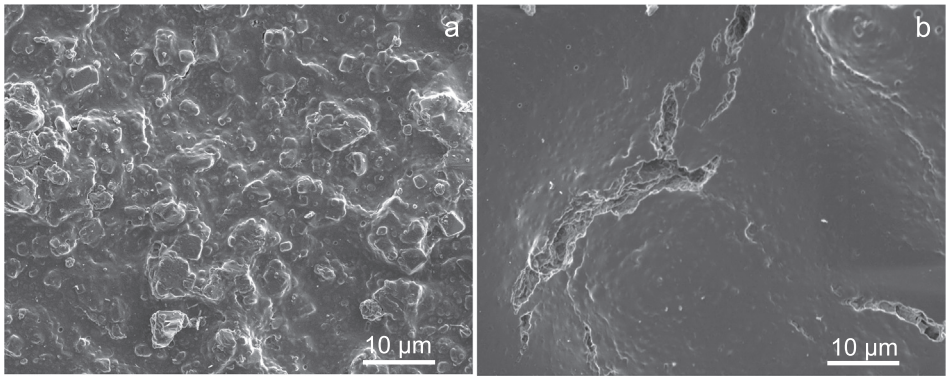

Fig. 5. SEM images of cinnabar and vermilion-based paint surface a) fine-grained VER-ST-EY and b) coarser-grained CIN-M-EY, showing important crack formation.

3.3. Weathering of HgS-based tempera paint surfaces

3.3.1. Microscopic observations of blank and aged paint dosimeters

Microscopic images revealed different alteration phenomena undergone by paints exposed to the various weathering tests (Fig. 6). For comparison an image of the blank dosimeter is included, which shows the presence of impurities, primarily composed of dark and colorless crystals (Fig. 6a, arrows). These crystals have been identified as sulfur-bearing minerals and quartz using FESEM (see above). Note that only images of CIN-M-EY and VER-ST-EY are included, which serve as representative examples for the different alteration processes undergone by HgS-based paints during the various aging tests.

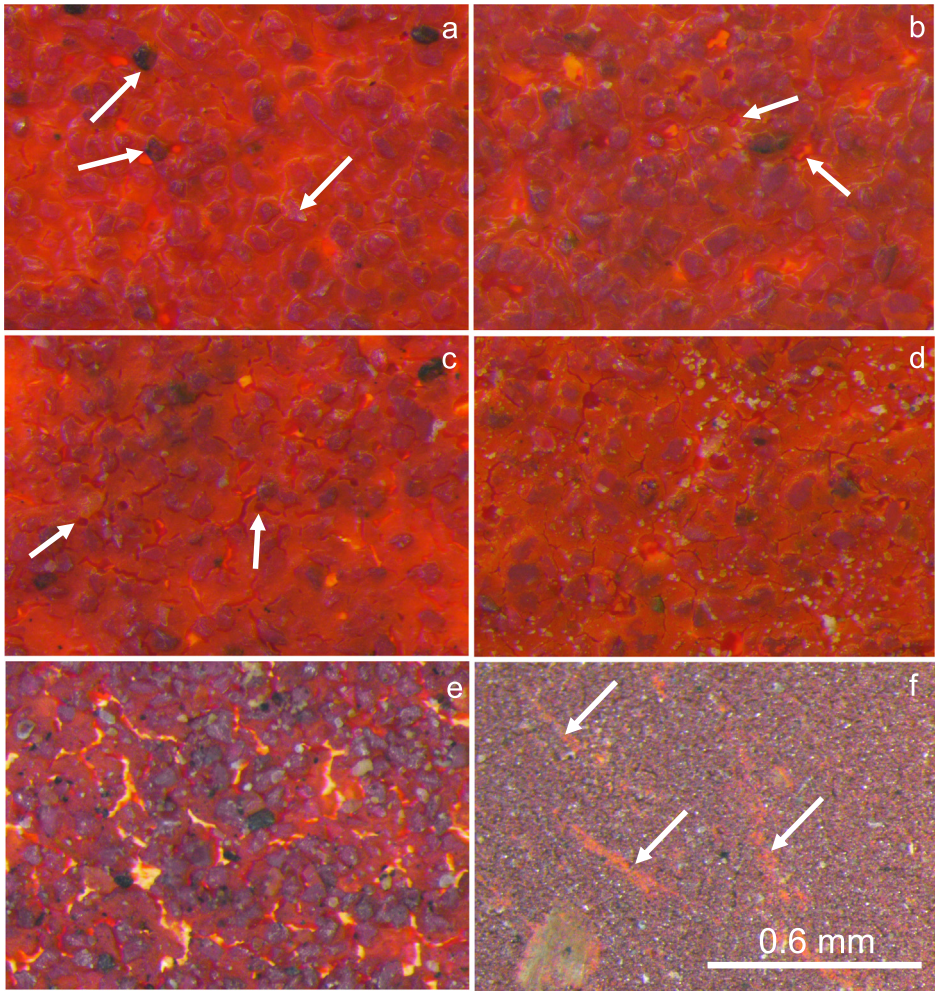

Fig. 6. Stereomicroscope photographs of cinnabar paint dosimeters (panels a–e. CIN-M-EY). a) Blank dosimeter (arrows showing dark and colorless crystals present as impurities in the original pigments); b) dosimeter showing surface pitting after RH cycling (arrows); c) UV-aged dosimeter suffering crack-formation, micro-pitting (arrows), and slight yellowing of the binder; d) dosimeter with surface deposition of white crystals after 2-year outdoor exposure at the Alhambra; e) dosimeter exposed in the city center for 2 years, suffering severe binder loss and darkening of the surface, and f) VER-ST-EY dosimeter exposed for 2 years in the city center, arrows indicate the scratched superficial alteration layer showing the original vermilion color underneath.

Table 3
Lightness (L*), a* and b* parameters, and chroma (C*) of blank dosimeters and dosimeters subjected to RH cycling, UV-, and 2-year outdoor exposure at the Alhambra (A) and in the city center (CC). Average values ± standard deviations are reported in consecutive rows.

	L*	a*	b*	C*	ΔL*	Δa*	Δb*	ΔC*	ΔE*
CIN-C-EY	42.08	33.57	23.49	40.97					
	±0.49	±0.44	±0.33	±0.54					
CIN-M-EY	43.50	34.48	23.59	41.78					
	±0.14	±0.44	±0.43	±0.60					
CIN-EF-EY	44.72	40.09	26.34	47.97					
	±0.32	±0.15	±0.54	±0.37					
VER-ST-EY	40.97	38.99	19.60	43.64					
	±0.15	±0.36	±0.27	±0.45					
CIN-C-EY-RH	42.01	34.31	24.31	42.05	−0.07	0.74	0.82	1.08	1.16
	±0.30	±0.30	±0.39	±0.46	±0.30	±0.30	±0.39	±0.46	±0.43
CIN-M-EY-RH	41.65	32.64	22.05	39.39	−1.85	−1.84	−1.54	−2.39	3.04
	±0.43	±0.40	±0.48	±0.60	±0.43	±0.40	±0.48	±0.60	±0.70
CIN-EF-EY-RH	44.30	39.65	25.39	47.08	−0.42	−0.45	−0.95	−0.89	1.23
	±0.21	±0.52	±0.71	±0.80	±0.21	±0.52	±0.71	±0.80	±0.74
VER-ST-EY-RH	40.47	38.95	19.66	43.63	−0.50	−0.04	0.07	0.00	0.61
	±0.16	±0.24	±0.25	±0.32	±0.16	±0.24	±0.25	±0.32	±0.12
CIN-C-EY-UV	42.78	34.98	24.61	42.77	0.70	1.41	1.12	1.80	1.96
	±0.23	±0.21	±0.27	±0.23	±0.23	±0.21	±0.27	±0.23	±0.26
CIN-M-EY-UV	42.64	35.08	23.78	42.38	−0.86	0.60	0.18	0.59	1.28
	±0.47	±0.43	±0.51	±0.64	±0.47	±0.43	±0.51	±0.64	±0.34
CIN-EF-EY-UV	44.39	39.93	25.35	47.30	−0.33	−0.17	−0.99	−0.68	1.14
	±0.23	±0.41	±0.24	±0.46	±0.23	±0.41	±0.24	±0.46	±0.26
VER-ST-EY-UV	40.30	41.20	22.43	46.91	−0.67	2.22	2.83	3.28	3.67
	±0.25	±0.19	±0.27	±0.28	±0.25	±0.19	±0.27	±0.28	±0.33
CIN-C-EY-A	42.71	29.85	21.27	36.65	0.63	−3.72	−2.22	−4.32	4.47
	±0.91	±0.50	±0.41	±0.56	±0.91	±0.50	±0.41	±0.56	±0.56
CIN-M-EY-A	43.35	31.98	21.64	38.61	−0.15	−2.51	−1.95	−3.17	3.19
	±0.23	±0.49	±0.17	±0.48	±0.23	±0.49	±0.17	±0.48	±0.47
CIN-EF-EY-A	44.28	39.91	25.83	47.54	−0.44	−0.19	−0.51	−0.44	0.78
	±0.27	±0.29	0.24	±0.36	±0.27	±0.29	±0.24	±0.36	±0.29
VER-ST-EY-A	40.70	39.45	20.26	44.34	−0.27	0.46	0.66	0.70	0.91
	±0.33	±0.13	±0.13	±0.17	±0.33	±0.13	±0.13	±0.17	±0.16
CIN-C-EY-CC	39.22	16.81	9.59	19.36	−2.86	−16.76	−13.90	−21.61	21.96
	±0.44	±0.35	±0.30	±0.29	±0.44	±0.35	±0.30	±0.29	±0.28
CIN-M-EY-CC	39.26	19.24	11.42	22.38	−4.24	−15.24	−12.17	−19.40	19.96
	±0.16	±0.11	±0.17	±0.14	±0.16	±0.11	±0.17	±0.14	±0.15
CIN-EF-EY-CC	40.25	20.86	10.05	23.16	−4.47	−19.23	−16.29	−24.82	25.60
	±0.02	±0.16	±0.05	±0.13	±0.02	±0.16	±0.05	±0.13	±0.10
VER-ST-EY-CC	38.98	18.11	6.25	19.16	−1.99	−20.87	−13.35	−24.48	24.86
	±0.25	±0.21	±0.09	±0.21	±0.25	±0.21	±0.09	±0.21	±0.22

CIN/VER-C/M/EF/ST = coarse, medium, extra fine, and standard cinnabar/vermilion; EY = egg yolk binder; UV/RH/A/CC = UV aging, RH cycling, and 2-year outdoor at the Alhambra or city center.

RH cycling under the exclusion of light (Fig. 6b) had hardly any negative effect on the paint surface and blackening was not detected. In a few cases, limited crack formation and surface pitting occurred.

UV-exposure primarily caused crack formation as a result of the low RH during the test (Fig. 6c), which was especially pronounced in coarse grained dosimeters. In a few cases, mainly in dosimeters containing fine grained pigments, surface pitting was observed, but blackening was not detected.

On outdoor-exposed dosimeters (Fig. 6d and e), deposition of predominately small white crystals on the paint surface was detected, which were identified as calcite/dolomite using XRD. Samples exposed for two years at the Alhambra suffered limited crack formation and surface pitting as a result of *T* and RH variations (Fig. 6d). However, pigment particles were still protected by the binder and only minor color change had occurred, which was confirmed by spectrophotometric results (see below). Paint dosimeters exposed in the city center of Granada suffered severe binder loss, especially in the case of coarse grained dosimeters, and the unprotected pigment particles now showed a superficial alteration layer of a grayish/violet color which caused an important darkening of the paint dosimeters (Fig. 6e). This alteration layer was relatively thin and the original color appeared after the surface was scratched with a diamond needle in the case of VER-ST-EY (arrow Fig. 6f).

3.3.2. Chromatic features of blank and aged paint surfaces

Color measurements were generally in good agreement with microscopic observations. The results (Table 3) revealed that blank dosimeters prepared with egg yolk and fine grained pigments (CIN-EF and VER-ST) were slightly more reddish and saturated (i.e., higher a* and C*) as compared to the ones prepared with coarser pigments (CIN-M and CIN-C). Parameters L* and b* were lowest in VER-ST-based paint and increased slightly with decreasing pigment grain size in the case of the Chinese cinnabar.

RH cycling only caused minor color changes (i.e., ΔE* ≤3 units) in dosimeters, which could not be correlated with particle size.

UV-exposure provoked color changes between 1.1 and 3.7 units. The most pronounced color change was observed in dosimeters prepared with VER-ST, which was predominately induced by an increase in a* and b*, suggesting a change towards a more reddish/yellowish color possibly caused by a yellowing of the binder upon UV exposure. Remarkably, this tendency was not observed in dosimeters prepared with CIN-EF, containing an even higher amount of binder as compared with VER-ST-based paint. The difference in behavior was likely related with the original pigment color, revealing a slightly more bluish shade in the case of VER-ST (Table 1), which was more affected by the yellowing of the binder.

Outdoor exposure caused very variable color changes depending on the prevailing environmental conditions at the location. At the

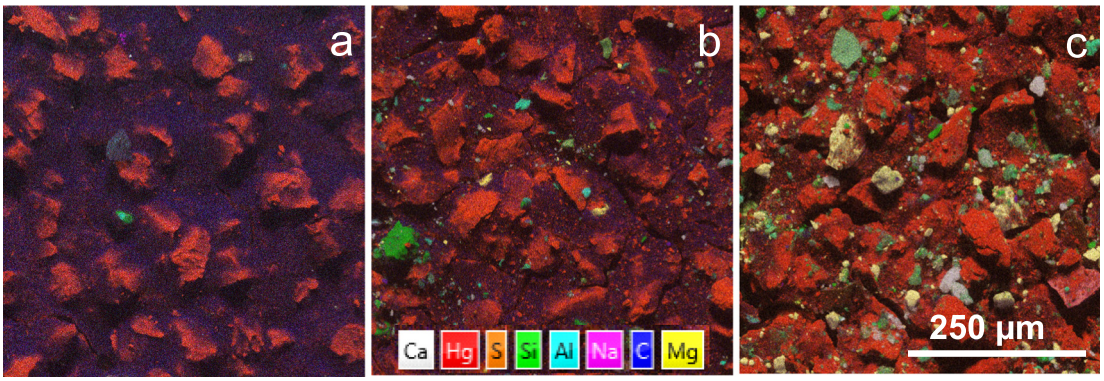

Fig. 7. FESEM elemental maps of CIN-M-EY paints: a) blank dosimeter and b) and c) dosimeters exposed for 2 years at the Alhambra and the city center, respectively, showing different degrees of surface soiling.

Alhambra, the coarse grained samples (CIN-M and CIN-C) exposed for 2 years suffered a color change of 3–4.5 units. This change was, generally, caused by a decrease in a* and b* suggesting a change towards green/blue. Surprisingly, dosimeters prepared with fine grained pigments (CIN-EF and VER-ST) did not experience important color change (i.e., ΔE^* <1 unit). Possibly, some yellowing due to binder degradation counteracted the decrease in a* and b* in fine grained paints. At the city center, blackening of cinnabar and vermilion was the prevailing cause of the dramatic color change between 17 and 25.5 units in dosimeters exposed for 2 years, reflected by an important decrease in L*, and especially in a* and b* (i.e., a color change towards green/blue and darkening). Color changes were, generally, slightly lower in dosimeters prepared with coarse pigments.

The results confirm stereomicroscopic observations, showing a significant darkening of HgS-based paint dosimeters exposed to direct sunlight in the city center of Granada. Remarkably, all pigments suffered severe color changes, including the vermilion from Almadén (Spain), which according to McCormack [10] would not undergo darkening. Samples exposed in the city center also experienced important binder loss and yellowing due to binder degradation was, thus, not observed. This is in contrast to the behavior of UV-aged dosimeters, which almost all suffered yellowing caused by the alteration of the binder (see ATR-FTIR results below).

3.3.3. Surface soiling and morphological changes upon outdoor exposure

A comparison of FESEM elemental maps of blank and outdoor exposed dosimeters prepared with coarse CIN-M pigment revealed an important difference in binder loss as well as surface soiling, which was especially evident in samples exposed at the city center (Fig. 7). Quantitative data (Table 4) showed a ~30 wt% reduction in C in the dosimeter exposed in the city center as compared to the blank dosimeter. Please note that the quantitative data should not be considered as absolute values but should only be used for comparison of different samples. In the case of the later, the C concentration only depended on the binder content. In the sample exposed in the city center, in contrast, the C concentration was also influenced by the deposition of carbonates and black carbon, which, in part, counteracted the decrease in C caused by binder loss and the actual binder loss might have been even higher. The increase in S and Hg in both outdoor-exposed dosimeters was a logical consequence of the binder loss, indicated by the decrease in C. Surface soiling was mainly due to the deposition of quartz, calcite, dolomite, aluminum silicates (clay minerals and feldspars (plagioclase)) and iron oxides/hydroxides which resulted in an increase in Si, Ca, Mg, Al, Fe, and O in the sample exposed at the city center and, to a lesser extent, in the one located at the Alhambra. Some of these minerals have been previously identified with XRD in outdoor-exposed dosimeters and are common constituents in soil dust at Granada [32,39]. Importantly, Cl was not detected in any of the analyzed HgS-based paints, which suggests that the darkening of cinnabar and vermilion pigments does not require halogens as catalysts.

FESEM images revealed that the prevailing environmental conditions during the 2-year outdoor exposure had an important influence on the final aspect of the paint surface (Fig. 8). Note that only dosimeters prepared with coarse CIN-C pigment are included which serve as representative examples. Images of unaltered CIN-C pigments are included for comparison (Fig. 8c and e). In the sheltered location at the Alhambra, pigment grains were still protected by the organic binder and the only detectable alteration phenomena were crack formation of the binder film (Fig. 8e, arrows) and limited deposition of soil dust. In the case of samples exposed at the city center important binder loss due to the direct action of sun and, more importantly, rain was detected (Fig. 8b). Some pigment grains showed thermal-induced crack formation caused by extreme diurnal temperature changes (Fig. 8b and d), being aggravated by direct sunlight exposure. It is very likely that heating was intensified by the darkening of the pigment grains over time. It is well established that black surfaces absorb more heat than lighter-colored ones [40]. Note that FESEM observations were directly performed on carbon-coated dosimeters and crack formation was no artifact of the sample preparation. The unprotected pigment grains in CIN-C-EY-CC were now covered with a superficial alteration layer composed of an aggregate of micron-size particles (Fig. 8d). These particles displayed a nanogranular structure, compatible with a dissolution-precipitation process, involving pseudomorphic phase replacement (Fig. 8f).

3.3.4. Changes in Hg/S ratio and Hg oxidation state upon outdoor exposure

XPS analysis of unaltered pigments showed that their surface was partially covered by a thin metallic Hg layer of a few nanometers. The binding energy of $Hg4f_{7/2}$ increased from initially 99.9 eV, value typically reported for Hg^0 [41], to 101.5 eV after 30 min ion-etching, roughly corresponding to 22.5 nm (Fig. 9a). This value is slightly higher than the value commonly reported for $Hg4f_{7/2}$ in cinnabar (i.e. 100.8 eV [41]). Quantitative compositional data corroborated the hypothesis that the pigment particle surface was enriched in Hg^0, revealing a decrease in Hg/S atomic concentration ratio from initially 1.38 to 1.02 after 30 min etching. The presence of a thin layer of metallic mercury on pigment

Table 4
Quantitative elemental composition (at.%) of the blank dosimeter and dosimeters exposed for 2 years at the Alhambra and in the city center based on FESEM high-resolution X-ray mapping.

Sample	C	O	Na	Mg	Al	Si	S	K	Ca	Fe	Ba	Hg
Blank	86.6	10.4	0.1	0.0	0.1	0.1	1.3	0.1	0.1	0.0	0.0	1.1
CIN-M-EY-A	80.0	14.3	0.2	0.1	0.1	0.3	2.0	0.1	0.3	0.0	0.0	1.7
CIN-M-EY-CC	59.8	26.6	0.1	0.7	0.7	1.6	4.5	0.1	1.5	0.4	0.1	4.1

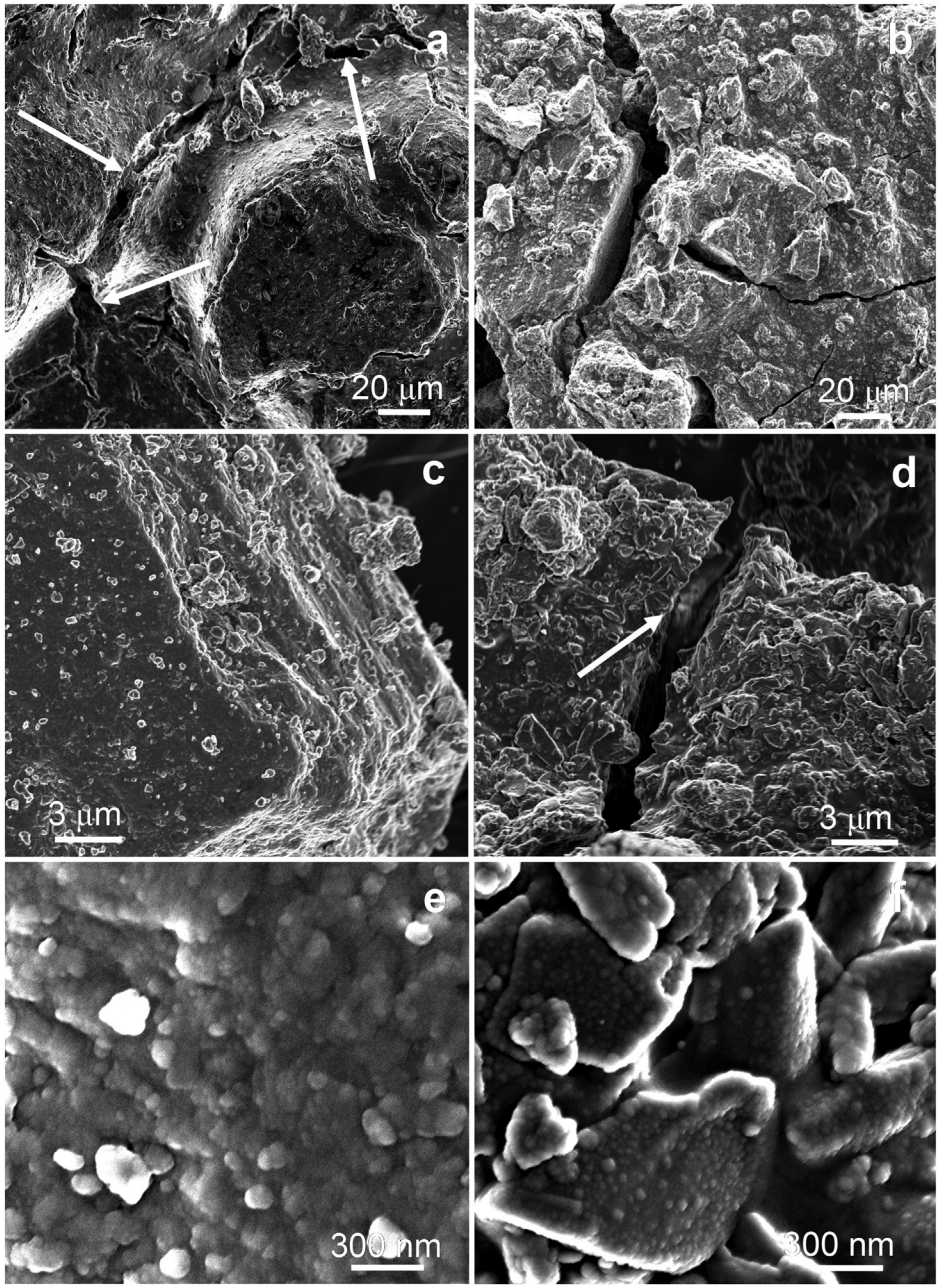

Fig. 8. FESEM images of cinnabar paints: a) CIN-C-EY-A exposed for 2 years at the Alhambra, showing severe crack formation of the proteinaceous binder (arrows); b) CIN-C-EY-CC exposed for 2 years at the city center, suffering binder loss and severe thermal-induced crack formation; c) unaltered CIN-C pigment; d) CIN-C-EY-CC, showing alteration layer and thermal-induced crack formation (arrow); e) detail of an unaltered CIN-C pigment grain surface, and f) detail of the alteration layer on CIN-C-EY-CC, displaying aggregates with a nanogranular structure on the crystal surface.

particles is consistent with microscopic observations in reflected light of the unaltered CIN-M-EY dosimeter, showing a metallic gloss on the surface of several pigments grains (Fig. 10a, arrows). Grains with metallic gloss can also be detected after 2-year outdoor exposure in the city center of Granada (Fig. 10b, arrows).

The results of XPS analysis of the CIN-M-EY-CC sample exposed for 2 years in the city center of Granada were less conclusive and revealed smaller changes in the Hg oxidation state upon ion etching as compared to the blank samples (Fig. 9b). The binding energy of $Hg4f_{7/2}$ in the upper-most layer (~7.5 nm) was 100.9 eV and decreased to 100.5 eV as the ion etching proceeded, which indicates a slight increase of the metallic Hg^0 component. Further ion etching (~67.5 nm nominal etch depth) caused a small blue shift of the $Hg4f_{7/2}$ binding energy to 100.9 eV, suggesting that the oxidized component (Hg^{+2}) increased again. According to Hsieh et al. [42] and Anaf et al. [13], oxidation of sulfur to SO_4^{-2} takes place during cinnabar degradation. XPS analyses, however, did not provide clear evidence for the formation of $HgSO_4$ in the case of the samples analyzed here. The binding energy of $S2p_{3/2}$ was 161.5 eV, a value typically reported for HgS [41].

When examining the XPS results of the outdoor-exposed dosimeter, the great inhomogeneity of the paints surface, which has been revealed by FESEM observations (i.e., the pigment surface being covered by an alteration layer, Fig. 8b), has to be taken into consideration. The obtained values for binding energies should be regarded as average values of the bulk surface, indicating a tendency rather than absolute values. Compositional data, however, provided clear evidence that the surface was

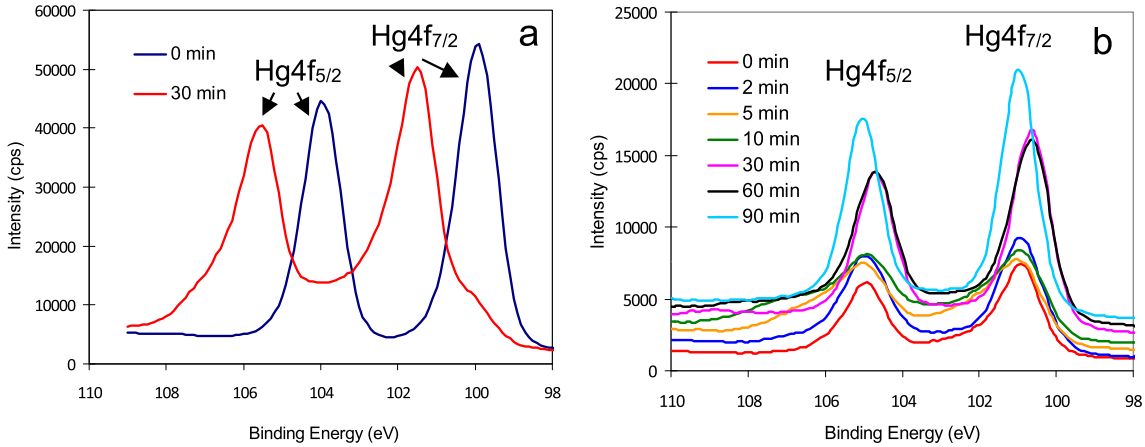

Fig. 9. Binding energy (eV) of $Hg4f_{5/2}$ and $Hg4f_{7/2}$ versus etch time (min) in a) CIN-M pigment, and b) CIN-M-EY-CC exposed for 2 years in the city center.

enriched in Hg (Fig. 11). The initial Hg/S ratio of the outermost altered paint surface was almost twice as high as that of the unaltered pigment. However, the Hg/S ratio decreased over time beyond the stoichiometric proportion of cinnabar. This decrease was likely caused by preferential Hg removal during Ar-etching [43]. The latter was corroborated by FESEM analysis, showing a significant modification of the surface impacted by ion etching (Fig. 1, Supplementary materials).

The presence of a metallic mercury layer on cinnabar is corroborated by several previous studies. Wang and Zhu [44] reported on XPS results, revealing a Hg-enriched surface layer with a Hg/S ratio of 1.3 on synthesized HgS nanoparticles. Furthermore, Strahan and Tsukada [45] demonstrated that Asian cinnabar lacquer objects released mercury vapor under controlled museum conditions, and McCarthy [46] reported on laboratory experiments which showed the presence of 0.04 mg/m^3 of mercury vapor over dry cinnabar at room *T*. In addition, mercury vapor emission has been associated with cinnabar deposits, released upon oxidation and weathering of ores [47]. In all these cases, the presence of metallic mercury is held responsible for the mercury vapor release. Note that the vapor pressure of mercury is 0.3 Pa at 25 °C [48] and it, thus, evaporates readily at room *T*.

Most probably, the formation of a metallic mercury layer on cinnabar and subsequent mercury evaporation are slow but continuous processes which also occur in the case of the unaltered pigment grains, though at a much lower rate. This hypothesis is in agreement with findings by Gustin et al. [49], who showed that some mercury emission from mercury compounds including HgS could be detected in the dark. Hg emission was, however, 1.5 to 116 times higher when the same compounds were exposed to daylight. Likely, blackening of HgS-based pigments and paints is only observed if a sufficiently large amount of metallic mercury accumulates on the pigment surface, probably bond via chemisorption. It seems plausible that the increased surface roughness of the altered cinnabar (Fig. 8b and c) in the case of outdoor exposed dosimeters at the city center facilitated the Hg adsorption. Overall, XPS results confirmed the presence of metallic mercury on outdoor-exposed darkened paint dosimeter as previously proposed by various researchers [11,13,19,20].

3.3.5. Conformational changes in the egg yolk binder upon weathering

According to ATR-FTIR results (Table 5), the amide I band of egg yolk at 1630 cm^{-1} with a shoulder at 1649 cm^{-1} can be assigned to a β-sheet structure with a contribution of a random coil component [50]. Conformational changes in egg yolk were neither detected after 1-month RH cycling, nor after 2-year outdoor exposure at the Alhambra (i.e., the amide I and II band positions remained unchanged). Accelerated UV-aging and outdoor exposure to direct sunlight in the city center, however, caused an important blue shift in the amide I band associated with an increase in the α-helix component at the expense of the β-sheet component [50]. The addition of cinnabar or vermilion to the egg yolk did not cause any significant changes in the conformational

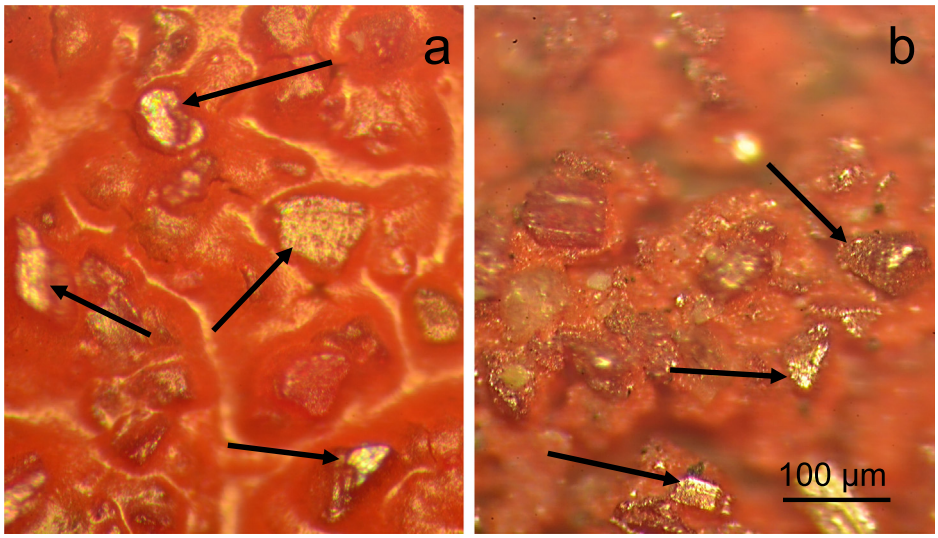

Fig. 10. Optical microscope images of a) unaltered CIN-M-EY, and b) CIN-M-EY-CC exposed for 2 years in the city center, showing pigment particles with metallic gloss.

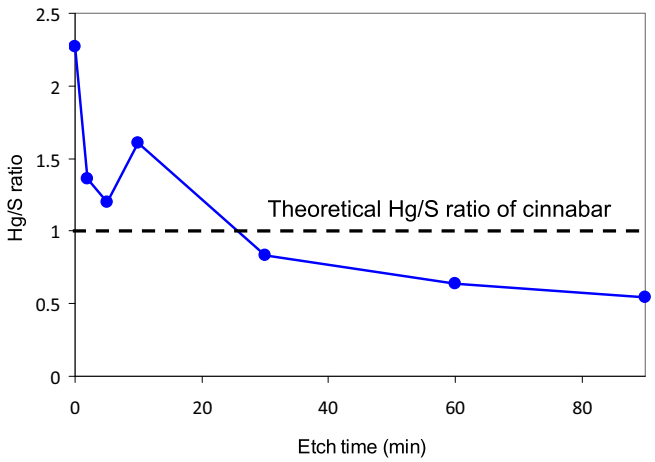

Fig. 11. Hg/S ratio versus etching time of CIN-M-EY-CC exposed for 2 years in the city center.

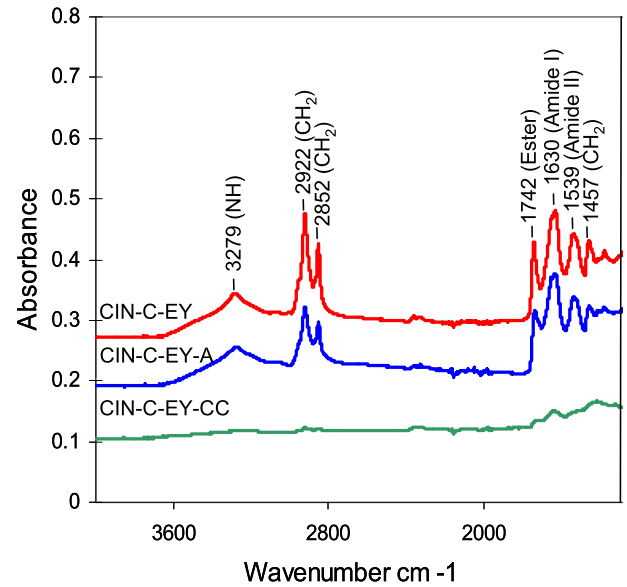

Fig. 12. ATR-FTIR spectra of blank and outdoor-exposed CIN-C-EY dosimeters, showing important binder loss indicated by a drastic intensity reduction of all characteristic bands of lipids and proteins in the sample exposed for 2 years in the city center.

structure of the binder (Table 5) and pigment-binder interactions did not seem to be influenced by pigment particle size in contrast to previous results, which showed stronger interactions as the particle size decreased in the case of azurite pigments [32].

Upon RH cycling and 2-year outdoor exposure in the absence of direct sunlight, the amide I band of paint dosimeters, in most cases, shifted to slightly lower frequencies without changing the conformational structure significantly. This shift became more pronounced with decreasing pigment particle size (Table 5). UV-exposure had a significant effect on the conformational structure of egg yolk-based paints, causing a blue shift of the amide I band. In the case of coarse-grained paint dosimeters (CIN-M and CIN-C), this shift can be related to a significant increase in the α-helix component. The blue shift in fine-grained paint dosimeters (CIN-EF and VER-ST) was smaller and indicates an important increase in the unordered, random coil component [50], which suggests a complete unfolding of polypeptide chains. After 2-year outdoor exposure in the city center no change of the amide I band position in paints prepared with coarse cinnabar pigments (CIN-M and CIN-C) was detected. Dosimeters prepared with fine-grained pigments (CIN-EF and VER-ST), in contrast, revealed a red shift of the amide I band, which, however, did not result in any significant conformational changes. Overall, the unsheltered dosimeters suffered important binder loss (Fig. 12), indicated by a dramatic intensity decrease of characteristic protein and lipid bands (i.e., amides and esters (triglycerides and phospholipids)).

The red shift experienced by the amide II band in cinnabar and vermilion-based paints upon accelerated UV exposure or direct sunlight exposure was likely the result of cross-linking and/or complexation of Hg^{+2} ions with the amide group. Note that complexation processes are known to reduce the frequency of the C—N bending vibrations as heavier atoms are attached [51,52] and UV-radiation has been successfully used to induce cross-linking in protein-metal complexes [53]. These results are in agreement with findings by Duce et al. [54], who also observed the formation of stable protein-pigment complexes and increased cross-linking upon aging of cinnabar tempera paint containing ovalbumin.

The ester band originally at ~1740 cm^{-1} in pure egg yolk and HgS-based paint shifted to slightly lower wavenumbers upon outdoor exposure/accelerated UV-aging. It has been previously reported that the aging of egg tempera especially affects triglycerides [55]. A similar shift has been reported by Meilunas et al. [56], who related this shift to the oxidation of triglycerides upon aging. In most cases, the ester/amide I band ratio decreased upon outdoor exposure/accelerated UV-aging (Table 5), indicating a decrease in triglycerides and phospholipids.

The experimental results indicate that pure egg yolk was more photo-sensitive as compared with rabbit glue binder, which was examined by the authors in a previous study [32]. Under identical weathering test conditions, no change in the amide I band position in rabbit glue was observed after UV- or 2-year outdoor exposure [32]. In the case of pure egg yolk, in contrast, UV/sunlight exposure caused important alteration in the conformational structure of egg yolk (i.e., the α-helix component increased significantly on the expense of the β-sheet component). Apparently, UV radiation induces photooxidation of organic compounds, involving the formation of radicals upon splitting of water molecules [57]. Contrary to rabbit glue, egg yolk not only contains proteins but also lipids (i.e., triglycerides, phopholipids, cholesterol, and cholesterol esters). Karpowiz [57] pointed to possible interaction

Table 5
ATR-FTIR data of ester, amide I, and amide II band position (cm^{-1}).

Sample[a]	Ester	Amide I	Amide II
Egg Yolk	1743	1630	1540
Egg Yolk-UV	1734	1658	1539
Egg Yolk-RH	1743	1629	1540
Egg Yolk-A	1740	1629	1541
Egg Yolk-CC	NA[b]	1652	1531
CIN-C-EY	1742	1630	1539
CIN-C-EY-UV	1733	1652	1533
CIN-C-EY-RH	1742	1630	1539
CIN-C-EY-A	1738	1630	1538
CIN-C-EY-CC	1733	1630	1526
CIN-M-EY	1741	1630	1539
CIN-M-EY-UV	1733	1651	1533
CIN-M-EY-RH	1740	1627	1539
CIN-M-EY-A	1734	1627	1539
CIN-M-EY-CC	1730	1635	NA
CIN-EF-EY	1740	1629	1538
CIN-EF-EY-UV	1734	1647	1533
CIN-EF-EY-RH	1740	1624	1538
CIN-EF-EY-A	1733	1626	1538
CIN-EF-EY-CC	1733	1620	1526
VER-ST-EY	1738	1627	NA
VER-ST-EY-UV	1733	1645	1528
VER-ST-EY-RH	1740	1626	NA
VER-ST-EY-A	1733	1622	NA
VER-ST-EY-CC	1736	1623	1526

[a] CIN/VER-C/M/EF/ST = coarse, medium, extra fine, and standard cinnabar/vermilion; EY = egg yolk binder; UV/RH/A/CC = UV aging, RH cycling, and 2-year outdoor at the Alhambra or city center.
[b] NA = not available.

between proteins and lipids in egg yolk, which caused protein degradation by peroxidizing lipids, indicated here by the red shift of the ester band (Table 5). These interactions are most likely responsible for the higher photo-sensitivity observed in egg yolk as compared to rabbit glue. The addition of coarse cinnabar pigment (CIN-M and CIN-C) to the egg yolk did not significantly influence the conformational changes undergone by the organic binder upon aging. However, finer grained pigments (CIN-EF and VER-ST) seemed to have provoked more important organic-inorganic interactions, which resulted in the oxidation of the organic binder, indicated by a complete unfolding of the polypeptide chains upon UV-aging [58]. Actually, several pigments are known to catalyze binder deterioration [59], and an increase in UV-induced oxidation in the presence of cinnabar has also been observed by Rasti and Scott [60] in the case of linseed oil-based paint and by Duce et al. [54] in the case of albumin-based tempera paint.

4. Conclusions

Analytical results revealed that neither UV radiation at low RH nor RH cycling under light exclusion induced darkening of HgS-based paints. Even prolonged outdoor exposure in a sheltered location at the Alhambra did not cause important color changes of the paint surface. After the above mentioned weathering tests, pigment grains were still covered by the egg yolk binder, which exerted a protective action against the photooxidation of cinnabar and vermilion. Severe darkening of the paint surface was only observed in dosimeters exposed to the direct action of sunlight and rain for 2 years. Here unfavorable environmental conditions resulted in an important binder loss as well as in compositional changes of the pigment surface layer. According to XPS analysis, the pigments´ surface layer was enriched in Hg, which confirmed the widely accepted hypothesis that a thin layer of metallic mercury is responsible for the darkening of HgS-based paints. In contrast to previous assumptions, the Hg-enriched surface layer formed in the absence of chloride, proving that the formation of metallic mercury was possible without the catalyzing action of halogens. Test results also showed that the darkening of cinnabar and vermilion was not influenced by the pigment's preparation process. Vermilion from Almadén, which seems to have been obtained by a wet-process, underwent similar alteration to that of ground Chinese cinnabar. Furthermore, XRD results suggest that both, vermilion from Almadén and cinnabar from China, likely contained some metacinnabar as impurity, which could be confused with an alteration product upon darkening.

Not only the paint's mineral component was affected by weathering processes, UV- and sunlight also caused significant conformational changes in the egg yolk binder, which imply that proteins and lipids underwent cross-linking and oxidation, in some cases accompanied by a slight yellowing of the binder. ATR-FTIR data also indicate the formation of protein-metal complexes. Generally, organic-inorganic interactions were stronger in paints prepared with fine grained pigments. Overall, the organic binder seemed to have acted as a physical barrier, protecting the cinnabar and vermilion pigment grains from light-induced photooxidation.

Changes in RH during accelerated and natural weathering caused important crack formation and surface pitting of the binder medium, which was especially pronounced in the case of paints prepared with coarse pigments. Additionally, the direct action of sunlight and rain over a prolonged period of time resulted in important binder loss, leaving pigment grains unprotected. The unprotected grains suffered thermal-induced crack formation due to severe temperature changes caused by the exposure to direct sunlight, which likely worsened as the pigment surface became darker during aging.

Finally, the deposited airborne particulate matter detected on outdoor-exposed paint dosimeters could act as catalyzing agents and contribute to photo-induced changes of cinnabar pigments. This aspect will be subject of future research.

Conflicts of interest

There are no conflicts to declare.

Funding

Financial support has been provided through the Research Projects AERIMPACT (CGL2012-30729) and EXPOAIR (P12-FQM-1889), funded by the European Regional Development Fund (ERDF), as well as by the Research Group RNM-179 (University of Granada). K. Elert was a postdoctoral fellow in the EXPOAIR Project (P12-FQM-1889).

Acknowledgements

FESEM and XPS analyses were performed at the “Centro de Instrumentación Científica” (CIC) of the University of Granada. We would like to thank I. Guerra and A. Herrera for the assistance with sample preparation and analysis.

Appendix A. Supplementary data

Supplementary data to this article can be found online at https://doi.org/10.1016/j.saa.2019.03.027.

References

[1] K. Hirst, Cinnabar - The Ancient Pigment of Mercury, http://www.thoughtco.com/cinnabar-the-ancient-pigment-of-mercury-170556, Accessed date: 3 October 2017.
[2] E.E. Bell, R.J. Sharer, L.P. Traxler, D.W. Sedat, C.W. Carelli, L.A. Grant, Tombs and burials in the early classic acropolis at Copan, in: E.E. Bell, M.A. Canuto, R.J. Sharer (Eds.), Understanding the Early Classic Copan, University of Pennsylvania Museum of Archaeology and Anthropology, Philadelphia 2004, pp. 131–158.
[3] M. Cotte, J. Susini, N. Metrich, A. Moscato, C. Gratziu, A. Bertagnini, M. Pagano, Blackening of Pompeian cinnabar paintings: X-ray microscopic analysis, Anal. Chem. 78 (2006) 7484–7492.
[4] C. Cardell, L. Rodríguez-Simón, I. Guerra, A. Sánchez-Navas, Analysis of Nasrid polychrome carpentry at the Hall of the Mexuar Palace, Alhambra complex (Granada, Spain), combining microscopic, chromatographic and spectroscopic methods, Archaeometry 51 (2009) 637–657.
[5] R.J. Gettens, R. Feller, W.T. Chase, Vermilion and cinnabar, Stud. Conserv. 17 (1972) 45–69.
[6] H.P. Schramm, B. Hering, Historische Materialien und ihre Identifizierung, VEB Deutscher Verlag der Wissenschaften, Berlin, 1988.
[7] S. Spring, R. Grout, The blackening of vermilion: an analytical study of the process in paintings, National Gallery Technical Bulletin, 23, 2002, pp. 50–61.
[8] R.L. Feller, Studies on the darkening of vermilion by light, Stud. Conserv. 1 (1967) 99–111.
[9] R.S. Davidson, C.J. Willsher, Mercury (II) sulphide: a photostable semiconductor, Nature 278 (1979) 238–239.
[10] J.K. McCormack, The darkening of cinnabar in sunlight, Mineral. Deposita 35 (2000) 796–798.
[11] F. Da Pieve, C. Hogan, D. Lamoen, J. Verbeeck, F. Vanmeert, M. Radepont, G. Van Tendeloo, Casting light on the darkening of colors in historical paintings, Phys. Rev. Lett. 111 (2013), 208302. .
[12] C. Hogan, F. Da Pieve, Colour degradation of artworks: an ab initio approach to X-ray, electronic and optical spectroscopy analyses of vermilion photodarkening, J. Anal. Atom. Spectrom. 30 (2015) 588–598.
[13] W. Anaf, K. Janssens, K. De Wael, Formation of metallic mercury during photodegradation/photodarkening of α-HgS: electrochemical evidence, Angew. Chem. Int. Ed. 52 (2013) 12568–12571.
[14] K. Keune, J.J. Boon, Analytical imaging studies clarifying the process of the darkening of vermilion in paintings, Anal. Chem. 77 (2005) 4742–4750.
[15] R.M. Dreyer, Darkening of cinnabar in sunlight, Am. Mineral. 24 (1939) 457–460.
[16] R.S. Davidson, C.J. Willsher, The light-induced blackening of red mercury (II) sulphide, J. Chem. Soc. Dalton Trans. (3) (1981) 833–835.
[17] R. Nöller, Cinnabar reviewed: characterization of the red pigment, Stud. Conserv. 60 (2013) 79–87.
[18] M. Radepont, Y. Coquinot, K. Janssens, J.-J. Ezrati, W. de Nolf, M. Cotte, Thermodynamic and experimental study of the degradation of the red pigment mercury sulfide, J. Anal. At. Spectrom. 30 (2015) 599–612.
[19] M. Radepont, W. de Nolf, K. Janssens, G. Van der Snickt, Y. Coquinot, L. Klaassen, M. Cotte, The use of microscopic X-ray diffraction for the study of HgS and its degradation products corderoite (α-$Hg_3S_2Cl_2$), kenhsuite (γ-$Hg_3S_2Cl_2$) and calomel (Hg_2Cl_2) in historical paintings, J. Anal. At. Spectrom. 26 (2011) 959–968.
[20] M. Kegelman Neiman, M. Balonis, I. Kakoulli, Cinnabar alteration in archaeological wall paintings: an experimental and theoretical approach, Appl. Phys. A Mater. Sci. Process. 121 (2015) 915–938.

[21] M. Price, A renaissance of color: particle separation and preparation of azurite for use in oil painting, Leonardo 33 (2000) 281–288.
[22] J. Romero-Pastor, A. Duran, A.B. Rodríguez-Navarro, R. Van Grieken, C. Cardell, Compositional and quantitative microtextural characterization of historic paintings by micro-X-ray diffraction and Raman microscopy, Anal. Chem. 83 (2011) 8420–8428.
[23] E.C.Y. Li-Chan, W.D. Powrie, S. Nakai, The chemistry of eggs and egg products (chapter 6), in: W.J. Stadelman, O.J. Cotterill (Eds.), Egg Science and Technology, The Haworth Press, Inc., New York 1995, pp. 105–175.
[24] M. Merrifield, Original Treatises on the Arts of Painting. v. I, Dover Publications Inc., New York, 1967.
[25] C. Cennini, The Craftsman's Handbook "Il Libro dell'Arte", Dover Publications Inc., New York, 1968.
[26] F. Pacheco, El arte de la pintura. Madrid: Cátedra, 1990.
[27] http://www.aemet.es/es/web/serviciosclimaticos/datosclimatologicos/valoresclimatologicos, Accessed date: 18 January 2017.
[28] Atlas, Weathering Testing Guidebook, Atlas Material Testing Technology, Illinois, USA, 2001.
[29] N. Velilla, www.ugr.es/~velilla/meteo-albayzin/resumen.htm, Estación meteorológica Granada-Albayzín, Spain (accessed 7.7.2016).
[30] J.D. Martín-Ramos, Using XPowder: A Software Package for Powder X-Ray Diffraction Analysis (GR 1001/04. ISBN 84-609-1497-6), 2004.
[31] R.S. Berns, Principles of Color Technology, 3rd ed. Wiley-Blackwell, Hoboken, 2000.
[32] C. Cardell, A. Herrera, I. Guerra, N. Navas, L. Rodriguez-Simon, K. Elert, Pigment-size effect on the physico-chemical behavior of azurite-tempera dosimeters upon natural and accelerated photo aging, Dyes Pigments 141 (2017) 53–65.
[33] C. Miguel, J.V. Pinto, M. Clarke, M.J. Melo, The alchemy of red mercury sulphide: the production of vermilion for medieval art, Dyes Pigments 102 (2014) 210–217.
[34] J. Viñalis Olia, C. Curto Mila, C. Nuñez Alvarez, Sobre la presencia de sulfuro de mercurio cubico (Metacinabrio) en el distrito minero de Almadén (Ciudad real, España), Treb. Mus. Geol. Barcelona 1 (1990) 209–218.
[35] A. Bernaus, X. Gaona, M. Valiente, Characterisation of Almadén mercury mine environment by XAS techniques, J. Environ. Monit. 7 (2005) 771–777.
[36] http://www.mindat.org/locentry-998545.html, Accessed date: 17 April 2017.
[37] H. Kühn, Erhaltung und Pflege von Kunstwerken und Antiquitäten 1. München: Keysersche Verlagsbuchhandlung, 1981.
[38] J.S. Pozo-Antonio, D. Barral, A. Herrera, K. Elert, T. Rivas, C. Cardell, Effect of tempera paint composition on their superficial physical properties-application of interferometric profilometry and hyperspectral imaging techniques, Prog. Org. Coat. 117 (2018) 56–68.
[39] M. Urosevic, A. Yebra-Rodríguez, E. Sebastián-Pardo, C. Cardell, Black soiling of an architectural limestone during two-year term exposure to urban air in the city of Granada (S Spain), Sci. Total Environ. 414 (2012) 564–575.
[40] D.E. Backenstow, Comparison of White vs. Black Surfaces for Energy Conservation. 8th Conference on Roofing Technology, 4, NCRA (National Roofing Contractors Association), Gaithersburg, 1987 16–17http://www.nrca.net/roofing/Eighth-Conference-on-Roofing-Technology-275, Accessed date: 6 February 2018.
[41] National Institute of Standards and Technology (NIST), https://srdata.nist.gov/xps/ElmSpectralSrch.aspx?selEnergy=PE, U.S. Secretary of Commerce, (accessed 10.2.2018).
[42] Y.H. Hsieh, S. Tokunaga, C.P. Huang, Some chemical reactions at the HgS(s)-water interface as affected by photoirradiation, Colloids Surf. 53 (1991) 257–274.
[43] C.R. Eddy, D. Leonhardt, V.A. Shamamian, J.R. Meyer, C.A. Hoffman, J.E. Butler, Characterization of the $CH_4/H_2/Ar$ high density plasma etching process for HgCdTe, J. Electron. Mater. 28 (1999) 347–354.
[44] H. Wang, J.J. Zhu, A sonochemical method for the selective synthesis of α-HgS and β-HgS nanoparticles, Ultrason. Sonochem. 11 (2004) 293–300.
[45] D. Strahan, M. Tsukada, Measuring mercury emission from cinnabar lacquer objects, Stud. Conserv. 61 (2016) 166–172.
[46] J.H. McCarthy, Mercury vapor and other volatile components in the air as guides to ore deposits, J. Geochem. Explor. 1 (1972) 143–162.
[47] K. Schlüter, Evaporation of mercury from soils: an integration and synthesis of current knowledge, Environ. Geol. 39 (2000) 249–271.
[48] J.F. Fisher, Elemental Mercury and Inorganic Mercury Compounds: Human Health Aspects. Concise International Chemical Assessment Document 50, World Health Organization International Programme on Chemical Safety, Geneva, 2003 (61 pp.).
[49] M.S. Gustin, H. Biester, C.S. Kim, Investigation of the light-enhanced emission of mercury from naturally enriched substrates, Atmos. Environ. 36 (2002) 3241–3254.
[50] J. Kong, S. Yu, Fourier transform infrared spectroscopic analysis of protein secondary structures, Acta Biochim. Biophys. Sin. 39 (2007) 549–559.
[51] S. Jhaumeer-Laulloo, M.G. Bhowon, K. Reddi, Synthesis and characterization of benzamide metal complexes, Asian J. Chem. 12 (2000) (1296e300).
[52] SIAS, Infrared Spectroscopy (IR), Royal Society of Chemistry, 2009.
[53] S.S. Wong, D.M. Jameson, Chemistry of Protein and Nucleic Acid Cross-linking and Conjugation, Taylor & Francis Group, Boca Raton, 2012.
[54] C. Duce, L. Ghezzi, M. Onor, I. Bonaduce, M.P. Colombini, M.R. Tine, E. Bramanti, Physico-chemical characterization of protein–pigment interactions in tempera paint reconstructions: casein/cinnabar and albumin/cinnabar, Anal. Bioanal. Chem. 402 (2012) 2183–2193.
[55] R. Mazzeo, S. Prati, M. Quaranta, E. Joseph, E. Kendix, M. Galeotti, Attenuated total reflection micro FTIR characterisation of pigment–binder interaction in reconstructed paint films, Anal. Bioanal. Chem. 392 (2008) 65–76.
[56] R.J. Meilunas, J.G. Bentsen, A. Steinberg, Analysis of aged paint binders by FTIR spectroscopy, Stud. Conserv. 35 (1990) 33–51.
[57] A. Karpowicz, Aging and deterioration of proteinaceous media, Stud. Conserv. 26 (1981) 153–160.
[58] S. Venkatesh, K.B. Tomer, J.S. Sharp, Rapid identification of oxidation-induced conformational changes by kinetic analysis, Rapid Commun. Mass Spectrom. 21 (2007) 3927–3936.
[59] W. Anaf, O. Schalm, K. Janssens, K. De Wael, Understanding the (in) stability of semiconductor pigments by a thermodynamic approach, Dyes Pigments 113 (2015) 409–415.
[60] F. Rasti, G. Scott, The effects of some common pigments on the photo-oxidation of linseed oil-based paint media, Stud. Conserv. 25 (1980) 145–156.